Deconvolution from instrumental devices and source effect in acoustic experiments

Henri-Pierre Valero, Stéphanie Gautier, G. Saracco, Matthias Holschneider

Deconvolution From Instrumental Devices and Source Effect in Acoustic Experiments

Henri-Pierre Valero, Stéphanie Gautier, Ginette Saracco, and Matthias Holschneider

***Abstract*—Two methods to deconvolve experimental data from the distortions introduced by instrumental devices or source effects are presented. Considering a total acquistion system (emission-reception line, amplifier, pre-amplifier) as a global experimental filter, we can define its properties (module and phase) experimentally from the generation of a family of source signals dilated in time. The estimation of this filter allows the deconvolution of the recorded output signal. The first approach is based on the simple reconstruction formula of the continuous wavelet transform (CWT). The second method is based on the construction of a normalized family of a finite number of specific filters, independent of the frequency range used. In both cases, experimental results in an acoustic tank are presented. We show that after deconvolution, the source signal is correctly reconstructed from the recorded output signal and the global instrumental filter.**

***Index Terms*—Acoustic experiment, continuous wavelet transform, deconvolution, diffraction tomography experiment, family of adapted and normalized filters, heterogeneous rock, simple reconstruction formula of the CWT, transmission experiment, ultrasonic data.**

I. Introduction

A signal measured by an instrumental device can be represented by the following equation:

$$O(t) = (F_{\text{ins}} * m * I)(t) \tag{1}$$

where F_{ins} corresponds to the response of the instrumental device, m to the impulse response of the medium and I to the input signal sent by the generator to the experimental system. O is the propagated signal measured by the receiver.

The problem to solve is therefore the following: Is it possible to get back the input signal $I(t)$ considering the effects of the different measurement devices. In fact, it is the same as doing the contrary operation of (1) which means a deconvolution.

Numerous deconvolution methods dealing with different problems and input parameters of the system exist ([1]–[4], [6]–[8], [12]). The most robust method is the Wierner-Levinson one ([5], [11]), where the filter is defined by the minimization of a quadratic form, namely the measurement error in the sense of the least squares method. Our approach consists in the following. We first build the global instrumental response of our device with the help of a test medium; then we apply its inverse to the measured output signals. These methods have been applied in real acoustic experiments for low ultrasound frequencies with omnidirectional transducers, and for high ultrasound frequencies with planar directional transducers. We will present the calculated filters as well as the deconvolved data of the instrumental response of the devices for two kinds of source signals.

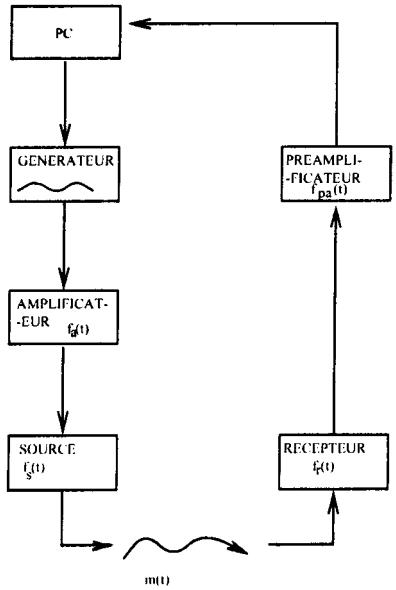

Fig. 1. Scheme of the experimental set-up in the water-tank.

II. Experimental Conditions

Different propagation experiments are performed in a water tank (dimension: $L \times P \times l = 2 \times 1.6 \times 1.5$ m) in the Acoustic Laboratory at Rennes, France. The scheme of the experimental set-up is presented in Fig. 1. Fig. 2 shows the comparison between the theoretical signal generated by the synthesizer which is sent to the source hydrophone, and the one recorded by the receiver after crossing the experimental device.

We can see that the device has an instrumental response variable with respect to the frequency range of the generated signal. The water creates only a time-delay dephasing, without dispersion effect, and the geometrical divergence of the omnidirec-

Manuscript received December 12, 2001; revised January 23, 2002. This work was supported by the CNRS and ANDRA through the GdR FORPRO (Research Action 2001/25A) and by the CPER with IFREMER Institute of Brest, France.

H.-P. Valero is with Schlumberger K.K., Sonic Interpretation, Interpretation Product Line, Sagamihara-shi, Kanagawa-ken, Japan (e-mail: valero@fuchinobe.skk.slb.com).

S. Gautier is with CNRS-Géosciences-Rennes, Géophysique Interne, Campus de Beaulieu, Rennes cedex, France (e-mail: gautier@univ-rennes1.fr).

G. Saracco was with CNRS-Géosciences Rennes, France. She is now with CNRS-CEREGE, Geophysics Department, Aix-en-provence cedex, France (e-mail: ginet@cerege.fr).

M. Holschneider was the with CNRS-Géosciences Rennes, France. He is now with Universtitat Potsdam, Applied and Industrial Mathematics, Potsdam, Germany (e-mail: hols@math.uni-potsdam.de).

Publisher Item Identifier S 0018-9456(02)04316-4.

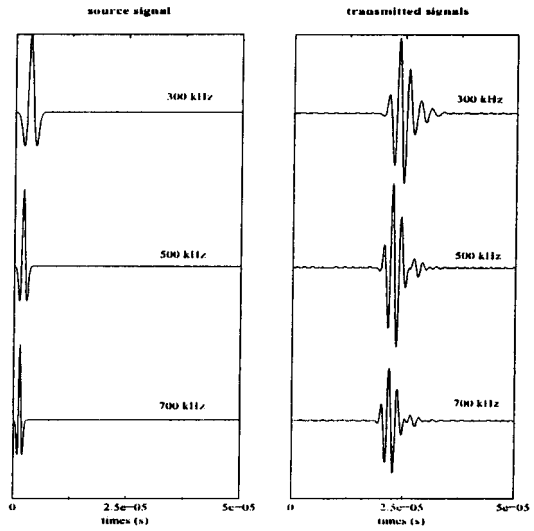

Fig. 2. Comparison of emitted source signal (left) and received signal after crossing the experimental device (right).

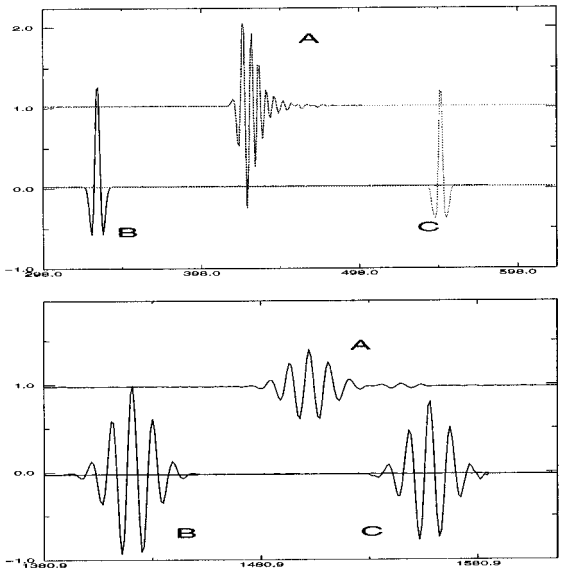

Fig. 3. Deconvolution examples for a Ricker (top) and a Morlet's wavelet (bottom) using the simple reconstruction formula of the CWT (first method). The curves represent respectively A: the signal measured to the receiver after crossing the experimental device, B: the source signal and C: the rebuilt signal.

tional transducer generates a weak absorption of sound during the travel of the wave between the two kinds of transducers.

Although all sensors have a limited frequency range, we have to choose this range in accordance to the geometrical and mechanical parameters that we want to study in real experimental applications. We need to keep a constant ratio between the geometrical dimensions and the wavelength of the source, if we want to transpose in acoustic laboratory experiments, real experimental conditions. Examples include the size of heterogeneities in front of the emitted wavelength in the diffusion problem, or the distance between the scatterer or the source with regard to the receiver in the propagation or scattering problem. Moreover, a transposition in low ultrasound frequencies implies multiple parasite reflections on the walls of the acoustic tank. These waves can be partially attenuated with the help of alveoled and conics absorbers (latex or polyethyrene material mixed to high density composites).

In geoexploration experiments, the frequency range currently used is around 0.1 Hz–10 kHz. This corresponds to a wavelength transposition of 100 m–1 dm in the acoustic tank respectively to a water mean velocity of 1500 m/s. To keep a constant ratio between the physical parameters to be analyzed and experimental geometric parameters, we need to work in a frequency range of 10 Hz–1 MHz. The limitations on one hand of tank dimensions and on the other hand of the piezoelectric technology imply working with two kinds of ultrasound source: a signal limited to a frequency-range of 20 kHz–140 kHz (omnidirectional transducer) and to ultrasound-range 100 kHz–1 MHz (directional transducer). This corresponds to a global wavelength of 15 cm to 0.15 mm.

III. Methods of Deconvolution

A. First Method

If $S(b,a)$ are the wavelet coefficients of the global instrumental filter $F_{\text{ins}}(t)$ associated to a dilated family of "wavelet-source" signals $(D^a I)(t)$, we can write under some conditions ([9], [10]) an exact formula allowing us to reconstruct for each time τ the global filter

$$F_{\text{ins}}(\tau) = R_e\left[K_I \int_0^{+\infty} S(\tau,a)\frac{da}{a}\right] \tag{2}$$

where K_I is a nonnull constant defined by $K_I = \int_0^{+\infty}(\hat{I}^*(u)/u)du$. I^* is the complex conjugate of the analyzing wavelet I such that

$$S(b,a) = (F * D^a\tilde{I})(b)$$

with $\tilde{I}(t) = I^*(-t)$. $\hat{I}$ is the Fourier transform of I.

The instrumental filter expression in this discrete form is then

$$F_i(t) = K_g \sum_{n=\min}^{\max} S_{F_n}(t,a_n)\frac{\Delta a_n}{a_n} \tag{3}$$

where $\min$ and $\max$ correspond to the minimal and maximal value of the emitted frequency. The fact of limitations on the number of dilation parameters may lead to a loss of information during the reconstruction of the filter. Nevertheless, it is necessary to apodize $\hat{I}^*(u)$ to obtain a good result in the time domain. This method which is easy to apply depends on the frequency range of the generated input signals. A necessary condition for the reconstruction is to generate a wavelet family with a scale-range of 3 octaves, decomposed linearly into 10 voices (linear intervals). It means that the result depends on the number of wavelets generated. Nevertheless, the results of the deconvolution with an apodization window show that the source signal is correctly reconstructed from the recorded transmitted signal and the instrumental global filter (see Figs. 3 and 4). These results are obtained in low ultrasound frequencies with omnidirectional hydrophones for two different transient signals: a Ricker function (derivative of second order of a Gaussian function) and

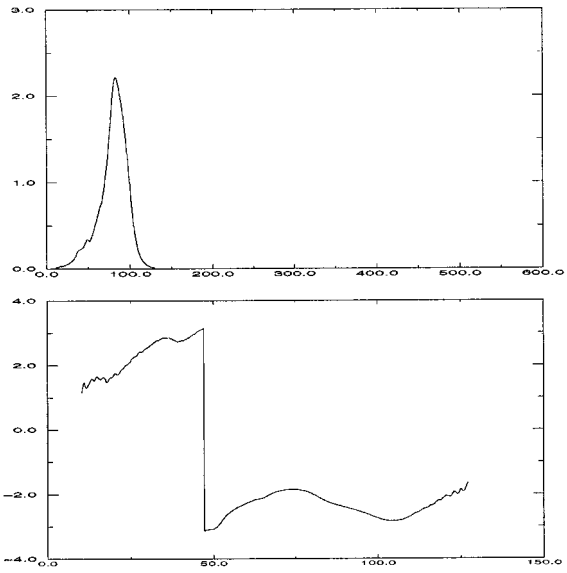

Fig. 4. Modulus and phase (un-wrapping) of the instrumental filter using the simple reconstruction formula of the continuous wavelet transform (first method).

a Morlet's wavelet (modulated Gaussian). The number of octaves of the dilation parameters is close to three (20–140 kHz). We can observe a weak difference in the amplitude between the input signal A and the reconstructed signal C. Nevertheless, the waveforms are correctly rebuilt.

B. Extended Method

Let us denote in Fourier space a general family of filters of controlled input signals $\hat{I}_n(u)$. After passage through the acquisition system we obtain, as previously, the measurements

$$\hat{O}_n(u) = \hat{F}_{\text{ins}}(u)\hat{I}_n(u).$$

Instead of recovering $\hat{F}_{\text{ins}}(u)$, we can only hope to obtain $\hat{\chi}(u)\hat{F}_{\text{ins}}(u)$, where $\hat{\chi}(u)$ is a suitable window function that we can choose such that

$$\sum_n (h_n * I_n)(t) = \chi(t).$$

We are looking for a solution

$$\hat{\chi}(u)\hat{F}_{\text{ins}}(u) = \sum_n \hat{h}_n(u)\hat{O}_n(u).$$

The filters h_n should be regular in order to obtain stable inversions. A solution to this problem is obtained by setting

$$\hat{h}_n(u) = \frac{\hat{I}_n^*(u)}{\sum\limits_m |\hat{I}_m(u)|^2} \times \hat{\chi}(u). \tag{4}$$

The main point is the choice of the function $\hat{\chi}$ which plays an important role in the stability of the calculus. This choice will be made by studying the behavior of the ratio

$$\frac{\hat{\chi}(u)}{\sum\limits_m |\hat{I}_m(u)|^2}. \tag{5}$$

A smooth and regular behavior of the ratio allows a limitation of the numerical instabilities in the computation of the individual filters when the denominator tends toward zero. It means we have to choose a function $\hat{\chi}(u)$ as the best fit of the total emitted energy

$$\sum_n |\hat{I}_n(u)|^2.$$

Two approaches are tested during acoustic experiments without and in the presence of scatterers (heterogeneous rock and plate of duralumin) with regard to the best fit of the total energy: a function $\hat{\chi}$ with a general predefinite shape (rectangular, Blackman or Kaiser Bessel window) and a function with an adapted shape.

The signal deconvolved for the voice n will be calculated as the following:

$$\hat{O}_n^d(u) = \hat{F}_{\text{inv}}(u)\hat{O}_n(u) \tag{6}$$

and

$$\hat{F}_{\text{inv}}(u) = \frac{\hat{\chi}'(u)}{\hat{F}_{\text{ins}}(u)} \tag{7}$$

where $\hat{\chi}'(u)$ is the adapted function deduced from $\hat{\chi}(u)$.

The deconvolved signal verifies:

$$\hat{O}_n^d(u) = \hat{\chi}'(u)\hat{I}_n(u). \tag{8}$$

So, we derive in fact a very general method of the construction of a filter appropriate to the experiment regardless of the input signal and the frequency range used.

IV. Application to Acoustic Data

A. Experimental Procedure in Water Tank Without Scatterers

Experiments are performed in two specified frequency ranges of 30 kHz–140 kHz with omnidirectional transducers and appropriate amplifier and pre-amplifier, and a frequency range of 200 kHz–1000 kHz with directional transducers for the extended method. The source signals emitted in the water tank are respectively a Morlet's wavelet

$$g(t) = \cos(u_0 t)\exp\left(-\frac{t^2}{2\sigma^2}\right) \tag{9}$$

and a Ricker's wavelet

$$r(t) = (1 - 2(\pi f t)^2)\exp((-\pi f t)^2). \tag{10}$$

Both families of functions are generated with a linear step: 10 voices per octave until 140 kHz with omnidirectional transducers and a regular step of 20 kHz in the second frequency range. This frequency range covers the band pass of the directional transducers of the central frequency of 500 kHz. The acquistion parameters (sampling frequency, voltage calibration, power gains for amplifier and preamplifier, …) are fixed during all the experiments. Consequently, the differences observed between the source emitted signal and the signal measured after propagation are only due to the global filter of the experimental devices.

1) The Simple Reconstruction of the Continuous Wavelet Transform (CWT) Method: The simple reconstruction formula

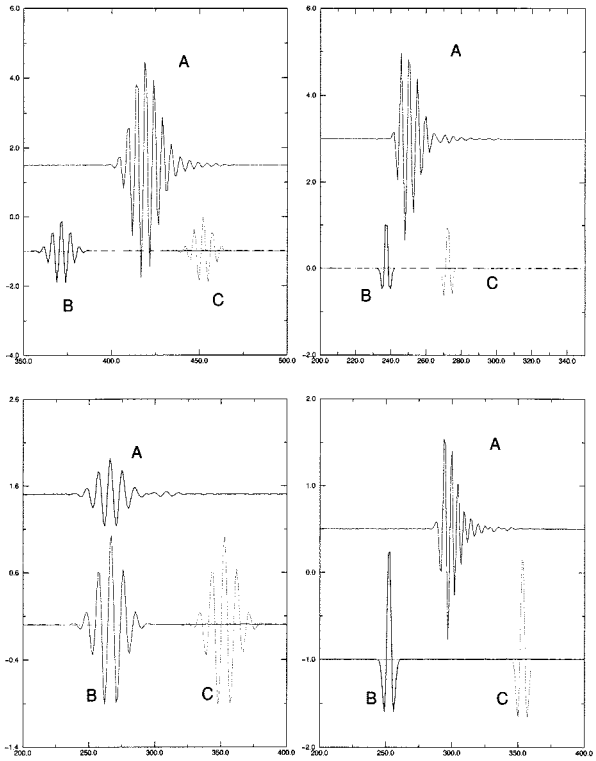

Fig. 5. Deconvolution examples based on the general method for a Ricker (right) and a Morlet's wavelet (left), for two different frequencies. The variations between the recorded signal, for two different frequencies, confirm the necessity to deconvolve data from the instrumental filter.

of the continuous wavelet method has been used to compute the experimental global filter thanks to water transmission experiments.

The results of the deconvolution in the case of the first method are shown (Fig. 3). The signal A corresponds to the output signal; B is the source signal generated by the synthesizer and sent to the emitter. C is the result of the deconvolution. The phasis and the modulus of the global instrumental filter are presented in Fig. 4 for an omnidirectional source and low frequencies, for a Ricker and a Morlet's wavelet. We can notice that the deconvolved signal C has a correct shape with regard to the theoretical signal source A, but its amplitude is weakly different (0.8% is lost). This difference of energy is due to the limitation of the voices introduced in the simple reconstruction formula of CWT, which covers slightly more than two octaves (30–140 kHz).

2) The Extended Method: This method has been applied to low frequencies with omnidirectional transducers with Ricker and Morlet's wavelet and to high frequencies with directional transducers in the case of Ricker's function. The characterization in both cases of the effects of instrumental devices on recorded signals is obtained by the construction of a finite number of individual and normalized filters independently of the frequency range used.

The deconvolution examples based on the extended method for omnidirectional transducers with a family of Morlet's function (left) and Ricker function (right) are shown in Fig. 5 with the same notation for the curves A, B, C as in Fig. 3. The predefinite shape of the window $\hat{\chi}'(u)$ used to obtain the best fit of the

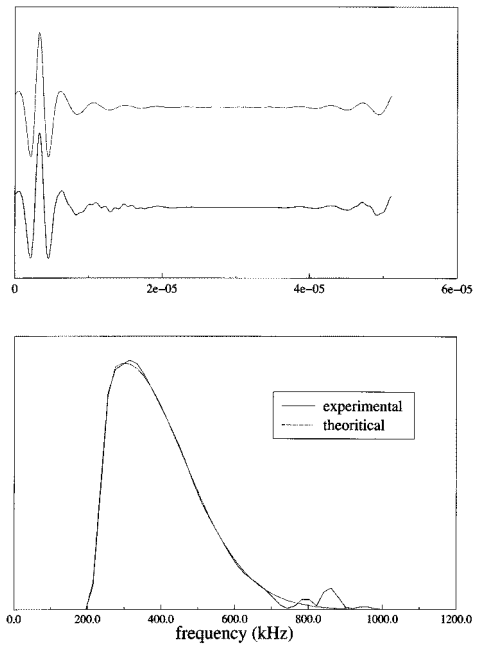

Fig. 6. Results from the deconvolution of recorded signal with inverse instrumental filter in time (top) and frequency domain (bottom) for the frequency source of 300 kHz.

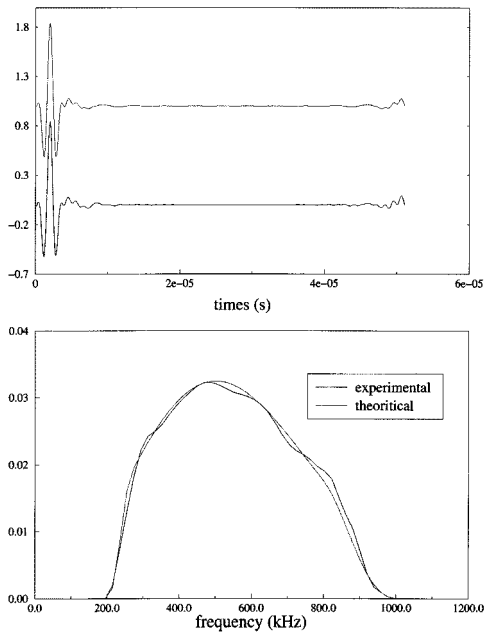

Fig. 7. Results from the deconvolution of recorded signal, in time (top) and frequency domain (bottom) for the frequency source of 500 kHz.

total energy [see (5)] is here the Hamming window. In this case, the amplitude and the waveform of the reconstructed signals C are in perfect concordance with the emitted signal A.

For directional transducers, the estimated global instrumental filter is shown in Fig. 11. Two examples of deconvolution are presented for a family of Ricker functions generated by transducers of the central frequency of $f_c = 500$ kHz, and deconvolved for a frequency source of $f_s = 300$ kHz (Fig. 6) and of $f_s = 500$ kHz (Fig. 7).

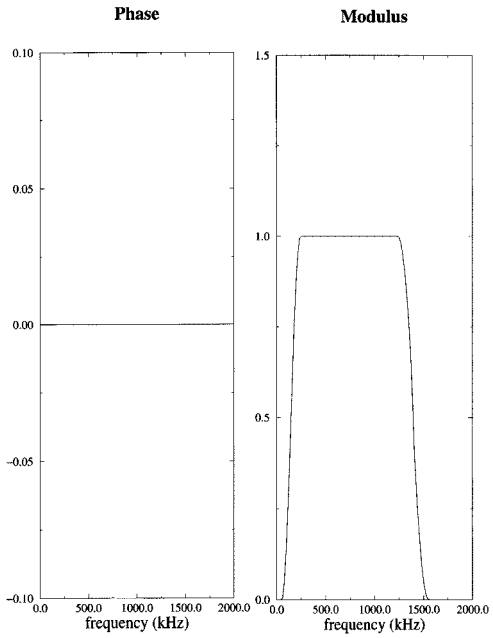

Fig. 8. Phase and modulus of the function $\hat{\chi}(u)$ used in the calculations.

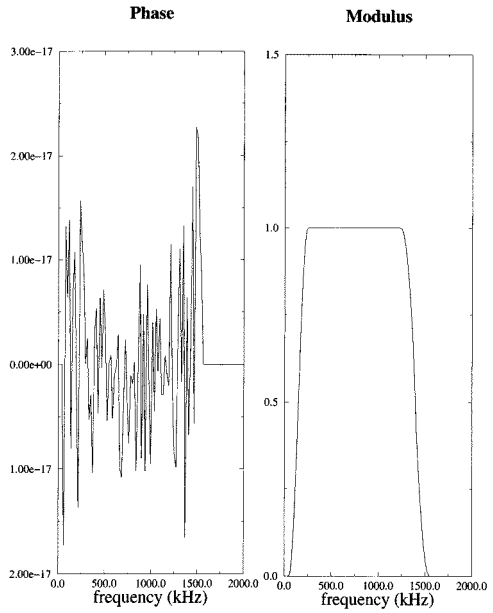

Fig. 9. Phase and modulus of the function $\hat{\chi}(u)$ rebuilt using Rickers as recorded data in the computation of the global filter.

The $\hat{\chi}(u)$ function used for the determination of the individual filters $\hat{h}_n(u)$ is initialized with a phase zero and an amplitude modulus of one. The characteristics of this function are presented in Fig. 8.

The adapted shape of the function $\hat{\chi}(u)$ allows limiting some numerical instabilities in the computation of the $\hat{h}_n(u)$ filters (Fig. 10). We verify the functions $\hat{\chi}(u)$ are well reconstructed (Fig. 9) using source signals as recorded signals in the computation of the instrumental filter. This good reconstruction is a proof of the precision of the method.

Fig. 11 shows the computed global filter of the experimental devices. The inverse global filter is then applied to the recorded signals in order to remove the effect of the instrumental filter

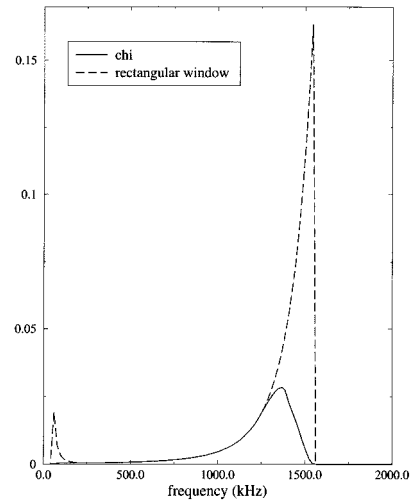

Fig. 10. Ratio modulus $\left(\hat{W}(u)/\sum_m |\hat{I}_m(u)|^2\right)$ for two kinds of window $\hat{W}(u)$: the function $\hat{\chi}(u)$ and a rectangular window with the same width. The regular behavior of the ratio when the window is the function $\hat{\chi}(u)$ indicates that the numerical instabilities are more limited than if we use the rectangular one.

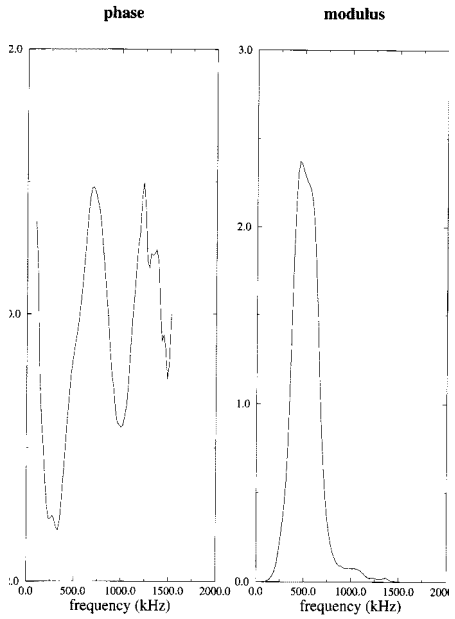

Fig. 11. Phase and modulus of the computed global instrumental filter.

from the data. The comparisons between the experimental results and the theoretical ones (source signal convolved with the $\hat{\chi}'(u)$'s function) are both in time and frequency domain, in a perfect concordance (Figs. 6 and 7). Some small high-frequency oscillations are present in the experimental curves. We can associate these small oscillations to the convolution of the transmitted signals with the inverse filter whose modulus reaches a maximum for these high frequencies. This method is nevertheless very efficient considering the weak differences between theoretical and rebuilt signals.

B. Experimental Procedure in Presence of Scatterers in the Water-Tank

In this section, the ability of the extended method to compute the filter in a more general experimental situation is tested.

Fig. 12. Diffraction tomography experiment with cylindrical rock immersed in the water tank and data acquisition system with hydrophones source and receiver.

We introduce different objects in the acoustic tank, and we try to evaluate the experimental response of these scatterers deconvolved from the instrumental device and/or the source.

In the first experiment, a cylindrical rock of lava (15 cm of diameter by 50 cm of length) is immersed vertically in the center of the water-tank. In order to image the whole lava sample, a pair of directional transducers (emitter–receiver) with an angular offset of 15 °, rotates around the target on a circle of 40 cm of radius from the center of the rotation axis (see Fig. 12). Seventy-two seismograms (or traces) per common-offset gather are recorded for a fixed depth z with the same source signal (Ricker function in time, i.e.,: second-order derivative of a Gaussian function), with an angular step of 5°. For each step we average over 16 recorded signals and one complete acquisition $(0 < \theta < 360°)$ takes around 8 min. These responses are recorded with a sampling rate of $4 \cdot 10^{-7}$ s and digitized by the A/D converter (5000 samples per trace), before being stored on the computer.

The whole lava sample is then targeted by a wave front issue from the directional source. Beforehand, the source signal is measured and recorded in the same conditions (sampling frequency, distance source receiver, temperature of water 20.2° and ambient noise) to perform a deconvolution of experimental data. Both transducers have a central frequency $f_c = 250$ kHz. The source-transducer will emit a family of Ricker functions toward the object in the frequency range of 100–400 kHz every 10 kHz up to the frequency of 130 kHz, then a step of 30 kHz up to the frequency of 400 kHz. The scattered pressure field is then measured by the second transducer.

The wavelength of investigation is between 1.48 mm and 0.37 mm in water with a water velocity of 1482.89 m/s [13] and attenuation coefficient $\alpha = 23 \cdot 10^{-3}$ Neper/m. These experiments need to have a good precision in translation 10^{-2} mm and in rotation 10^{-2} degree.

1) The Blackman Adapted Window: Two approaches are tested during this study: a function $\hat{\chi}'(u)$ with a general shape (rectangular and Blackman window). We present only results

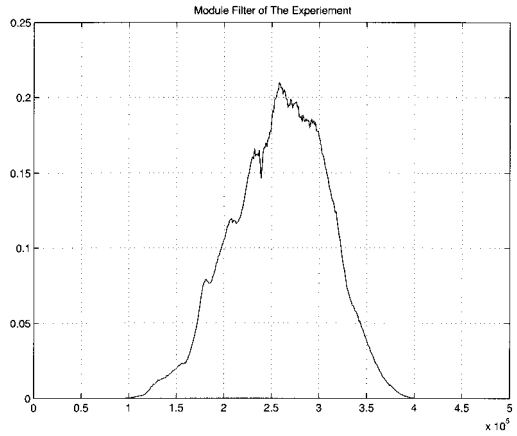

Fig. 13. Module of the experimental filter using the extended method without adaptive window, but with a shape of Blackman window.

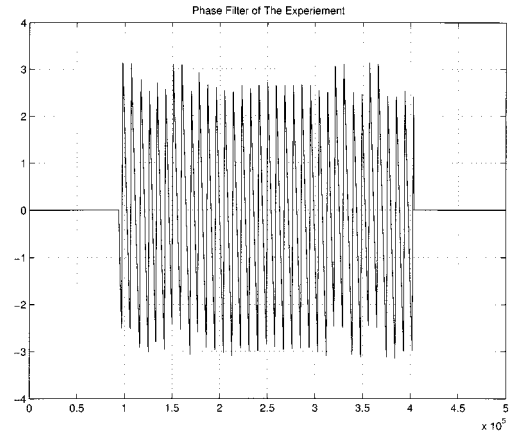

Fig. 14. Phase (un-wrapping) of the experimental filter using the extended method without adaptive window, but with a shape of Blackman window.

obtained with the extended method using a predefinite window with a fixed shape (Blackman function), but the support of the window is evaluated with regards to the best fit of the total emitted energy $\sum_n |\hat{I}_n(u)|^2$ and by studying the ratio in (5), in a diffraction tomography experiment.

Figs. 13 and 14 present the result of the experimental filter with Blackman window. It is interesting to notice that the variation of the amplitude, with respect to the frequency, points out the fact that this rock is clearly heterogeneous. This kind of methodology is really important to know the frequency behavior of rheological parameters of the rock as the intrinsic attenuation factor (attenuation in accordance with a Kelvin–Voigt model or a Maxwell model).

The rebuilt function $\hat{\chi}(u)$ corresponding to the Blackman adapted window using Ricker source signals as recorded signals in the computation of the global filter is presented in Fig. 15 for the modulus and Fig. 16 for the phase. These results correspond to the test that we perform since we have the h_n filters [see (4)] to verify that the reconstruction is correct. The adapted Blackman window can be defined. Fig. 18 represents the total emitted energy $\sum_n |\hat{I}_n(u)|^2$ and the study of its inverse allows defining the $\hat{\chi}(u)$ (adapted Blackman window) in order that the deconvolution be stable.

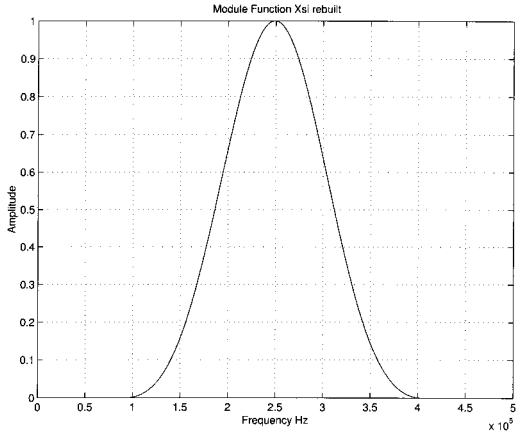

Fig. 15. Module of the $\hat{\chi}(u)$ function rebuilt using Rickers as recorded data in the computation of the global filter for the extended method with a Blackman adapted window.

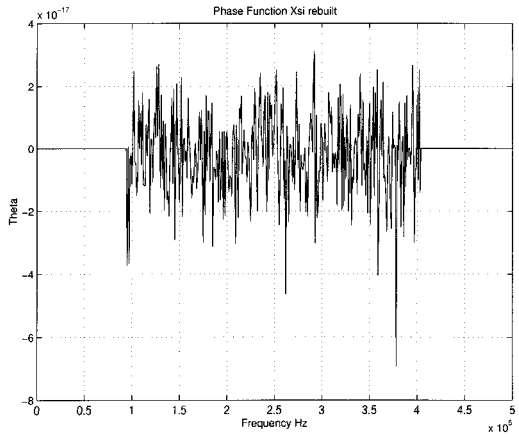

Fig. 16. Phase of the $\hat{\chi}(u)$ function rebuilt using Rickers as recorded data in the computation of the global filter for the extended method with a Blackman adapted window.

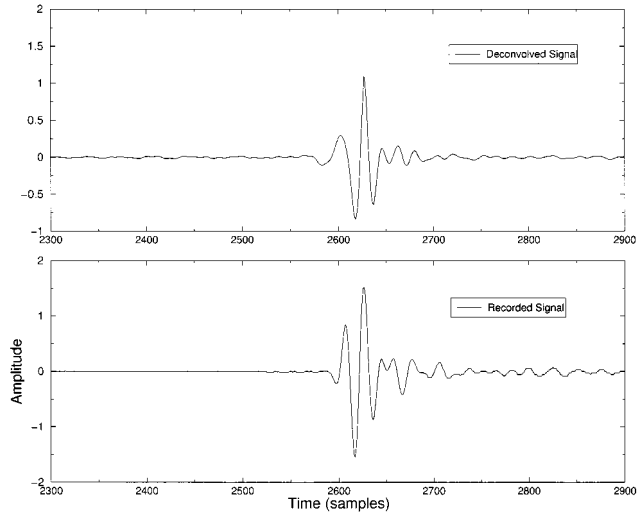

Fig. 17. Result after deconvolution of diffraction tomography data. One trace is presented using a Blackman adapted window with the extended method. The present distortions in the deconvolved signal are only due to the intrinsic attenuation of the rock. The effects of the source and of the instrumental devices are cancelled.

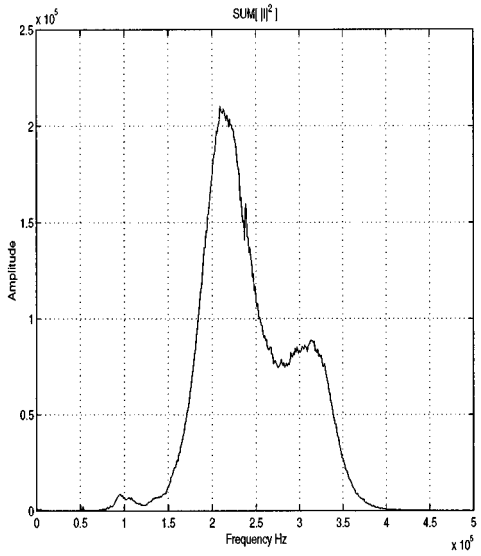

Fig. 18. Denominator of the hn function in (4) corresponding to the total emitted energy during diffraction tomography experiment for one azimuthal acquisition (or trace).

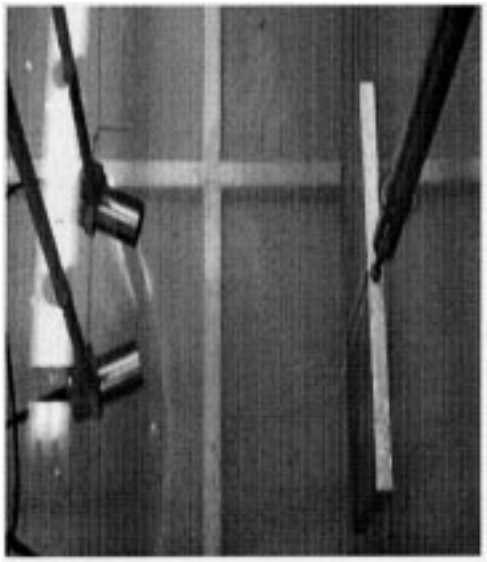

Fig. 19. Photography of the reflection experiments with the directional transducers and the plate of duralumin.

The result of the application of the inverse global filter on scattered field pressure is presented in Fig. 17. We can compare the experimental scattered field (one trace) recorded to the receiver-hydrophone (bottom), and the experimental scattered field after deconvolution of the instrumental device effect and source effect (top). The difference between these two signals is only due to the intrinsic attenuation properties of the lava sample.

2) The Adapted Function $\hat{\chi}(u)$: We have also attempted the extended method with the adapted function $\hat{\chi}(u)$ to build the experimental global filter with reflection measurements. A photograph of the reflection experiments is shown in Fig. 19. A perfectly reflecting plate made in duralumin is immersed in the water-tank. The directional source-transducer sends the same family of Ricker's wavelet as previously seen in Section IV-A. The receiver measures the reflected pressure field by the plate,

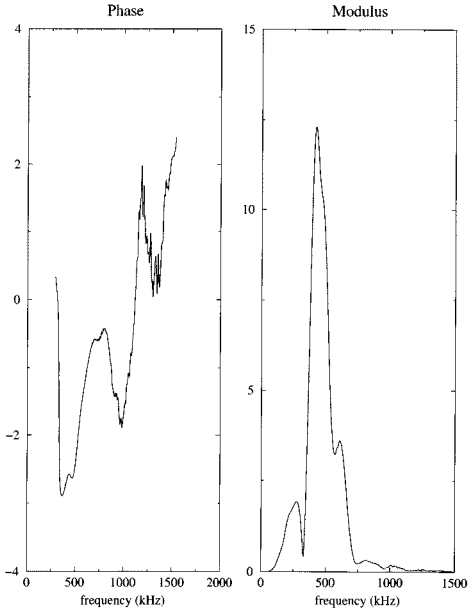

Fig. 20. Phase and modulus of the global filter in the case of reflection experiments.

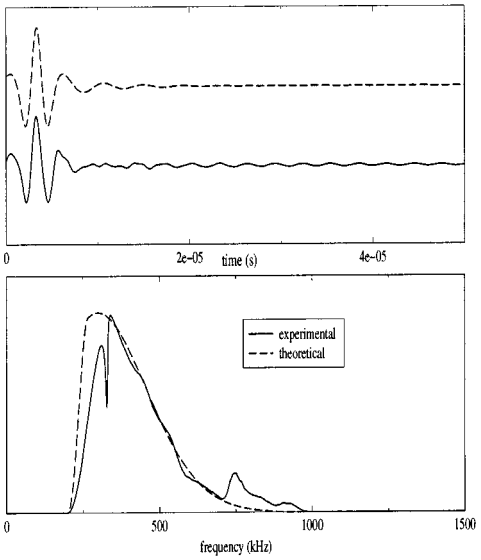

Fig. 21. Results from the deconvolution of reflected signal with inverse instrumental filter in time (top) and frequency domain (bottom) for the frequency source of 300 kHz.

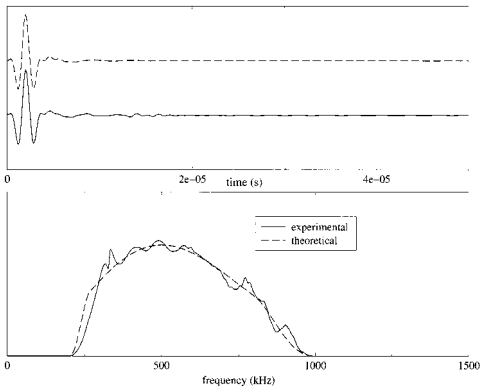

Fig. 22. Results from the deconvolution of reflected signal, in time (top) and frequency domain (bottom) for the frequency source of 500 kHz.

and this one is recorded and digitized (5000 samples) in order to be treated. The global filter estimated with the extended method is presented in Fig. 20.

We observed a good agreement between the deconvolved signals and the theoretical ones (Figs. 21 and 22). Nevertheless, we point out more important differences than with the water transmission experiments. These additional oscillations may be due to scattering resonances of the plate. These scattering resonances can also explain the local minima observed in the modulus of the global filter (Fig. 20).

V. Conclusion

These methods presented to build the global instrumental filter, and more general filters, are easy to implement from an experimental point of view as well as from a numerical one. They give similar results. The first one, based on the wavelet theory and more precisely on the simple reconstruction formula of the wavelet transform, depends on the dilation range generated. It means that the amplitude of the reconstructed signal can be lower than the emitted signal, because we need to have a minimum frequency range of three octaves during experiments. These conditions limit the efficiency of this method in laboratory experiments, in particular, in the acoustic tank. The second one, more general, is based on the construction of a family of filters that enables freeing ourselves from the work frequency range.

Acoustical experiments have shown the validity of both methods because of the good deconvolution of measured output signals. We notice that the extended methods are efficient independently of the emitted signal (Morlet or Ricker's functions), the directivity of the tranducers, the geometry of the acquisition system, and the frequency of the source signal compared with the central frequency of the transducers.

A new interest is the use of the presented methods to compute more general filters in the case of real experimental conditions for heterogeneous rock or a perfect reflector inserted in the middle of the tank. The two examples treated in this paper show the interest of these extended methods to deconvolve experimental data from the instrumental device and/or from the source effect, and where the energy after deconvolution is respected with regard to the frequency range of the source signal.

Acknowledgment

We want to thank M. LeMoine and F. Conil for their help and collaboration in the tomography experiments and reflection experiments. We also thank J. Lancelot and Ph. Lebon for their strong support since the beginning of this project.

References

[1] A. J. Berkhout, "Least-squares inverse filtering and wavelet deconvolution," *Geophysics*, vol. 42, pp. 1369–1383, 1977.
[2] N. Ott and H. G. Meder, "The Kalman filter as prediction error filter," *Geophys. Prospect.*, vol. 20, pp. 549–560, 1972.
[3] K. L. Peacok and S. Treitel, "Predictive deconvolution: Theory and practice," *Geophysics*, vol. 34, pp. 155–169, 1969.
[4] S. Treitel and L. R. Lines, "Linear inverse theory and deconvolution," *Geophysics*, vol. 47, no. 8, pp. 1153–1159, 1982.
[5] A. Jurkevics and R. Wiggins, "A critique of seismic deconvolution methods," *Geophysics*, vol. 49, no. 12, pp. 2109–2116, 1984.
[6] N. G. Paulter, "A causal regularizing deconvolution filter for optimal waveform reconstruction," *IEEE Trans. Instrum. Meas.*, vol. 43, Apr. 1996.

[7] S. Roy and M. Souders, "Non-iterative waveform deconvolution using analytic reconstruction filters with time-domain weighting," in *17th IEEE Instrum. Meas. Tech. Conf.*, vol. 3, 2000, pp. 1429–1434.
[8] T. J. Ulrych, "Application of homomorphic deconvolution to seismology," *Geophysics*, vol. 36, pp. 650–660, 1971.
[9] G. Saracco and P. Tchamitchian, "Retrieval of a time-dependent source in an acoustic propagation problem," in *Inverse Methods in Action (Inverse Problems)*, P. C. Sabatier, Ed. New York: Springer-Verlag, 1990, pp. 207–211.
[10] G. Saracco, P. Tchamitchian, and C. Gazhanes, "Transmission through a diopter and reconstruction of the source signal," *Coll. de Phys., 1st Cong. Franç. d'Acoust.*, vol. 2, no. 51, Les Edit. de Phys., pp. 1049–1052, Feb. 1990.
[11] E. A. Robinson and S. A. Treitel, "Principles of digital wiener filtering," *Geophys. Prospect.*, vol. 15, pp. 311–333, 1967.
[12] R. Wiggins, "Minimum entropy deconvolution," *Geoexploration*, vol. 16, pp. 21–35, 1978.
[13] M. Greenspan and C. E. Tschiego, "Tables of speed of sound in water," *J. Acoust. Soc. Amer.*, vol. 31, no. 1, pp. 75–80, 1959.

Henri-Pierre Valero received the Ph.D. degree in geophysics from the Institut de Physique du Globe de Paris (IPGP), Paris, France, in December 1997, sent on secondment to the CNRS-Geophysics Department of Rennes, France, where he developed seismic endoscopy to obtain azimuthal images around the borehole in the acoustic laboratory of Rennes under the guidance of G. Saracco and D. Gibert.

His work at the University of Rennes required the development of an experimental probe with acquisition hardware. The algorithms and software related to the proposed method were also implemented. From 1994 to 1995 he worked in CNES (National Spatial Center), Toulouse, France, in the Geodesic Department under the direction of A. Cazenave. The study concerned the computation of a high resolution geoid using ERS1 (orbit 35 days). In march 1998, he joined Schlumberger-Doll as an Engineer and now works in the Sonic Interpretation Department, Tokyo, Japan. His current interest is in acoustic wave propagation in boreholes and the application of signal processing to the data.

Dr. Valero is member of SEG and SPWLA.

Stéphanie Gautier received the M.S. in geophysics in 1999 from the University of Rennes I, Rennes, France. While studying for the M.S. degree, she worked on the propagation of the ballistic component of acoustic waves through sand samples (granular medium). She has been pursuing the Ph.D. degree in the Geophysics Department of CNRS-UMR 6118, University of Beaulieu (Rennes I), since 1999.

She now works on the characterization of rough discontinuities from acoustic backscattering experiments on granit and synthetic rock samples and has focused her interests on the acquisition of experimental data in an acoustic tank, the development of signal processing to extract the properties of rough interfaces from data, and the development of numerical algorithms to valid the methods. Her current research interests are in geophysical imaging, wave propagation in random media, and the application of signal processing on experimental data.

Ginette Saracco received the Ph.D. degree in propagation of transient acoustic signals (asymptotics methods and wavelet transform) in 1989.

She has been a Researcher since 1994 with the CNRS-Geophysics Department, Rennes, France. From 1986–1992, she was with the CNRS-Laboratory of Mechanics & Acoustics, Marseille, France, and in collaboration with A. Grossmann and Ph. Tchamitchian from the Center of Theoretical Physics, (CPT), Marseille-Luminy. For six months in 1986, she worked as Engineer of Research for Cap Sesa and Digilog Company detached in Naval Laboratory on signal processing using the continuous WT, then at the CNRS-LMA until 1992, on WT applied to underwater acoustics. She was an Associated Researcher for one year at Pennsylvania State University, State College, in the Applied Research Laboratory, she worked since 1994 at CNRS-Rennes on geohysical imaging, wave propagation in heterogeneous media, geomagnetic fields (jerks), inverse problems in potential fields, and acoustic tomography. She currently works with the CNRS-CEREGE, Aix-en-Provence, France, on inverse problems of self-potential tomography of porous heterogeneous medium and on the volcano-electric effect.

Matthias Holschneider received the Ph.D. degree in theoretical physics from the Center of Theoretical Physics, Marseille (CPT), France, in 1986, under the guidance of Alex Grossmann.

From 1987–1997, he held a research position in the CNRS-CPT, Marseille-Luminy, France, and from 1991 to 1993, he was a Buisiness Consulant for McKinsey an Co., Berlin, Germany. From 1997–1999, he worked in geophysics at the Institut Physique du Globe (IPGP), Paris, France, and in collaboration with the Géophysique Department of Rennes, France. He became Director of Research in 1999 of the CNRS in Géophysique area and worked from 1999 to August 2001 with the CNRS-Géophysique Department of Rennes on some applications of wavelet transforms in geophysical signal processing. Currently, since September 2001, he holds the chair of Applied Mathematics at the University of Potsdam, Potsdam, Germany, where he also is the director of the Applied and Industrial Mathematics Department.